Scalvenzi, M., Gargiulo, S., Freddi, F., Parisi, F. (2022). Impact of seismic retrofitting on progressive collapse resistance of RC frame structures. Engineering Failure Analysis, 131: 105840. https://doi.org/10.1016/j.engfailanal.2021.105840.

Impact of seismic retrofitting on progressive collapse resistance of RC frame structures

Martina Scalvenzi[1], Sebastiano Gargiulo[1], Fabio Freddi[2], Fulvio Parisi[1*]

[1] *Department of Structures for Engineering and Architecture, University of Naples Federico II, Naples, Italy*
[2] *Department of Civil, Environmental & Geomatic Engineering, University College London, London, United Kingdom*

Abstract

Most of the existing buildings in seismic prone regions have been built before the publication of modern design provisions against earthquakes, resulting in the need for structural retrofitting. Furthermore, some of those buildings are also subjected to additional hazards that may be either triggered by earthquakes (*e.g.*, landslides, soil liquefaction, tsunamis) or associated with other natural or anthropogenic events, such as floods, vehicle collision, blast, and fire. A multi-hazard performance assessment of building structures is thus of paramount importance to implement integrated retrofit strategies, which otherwise would not be economically sustainable if oriented to structural risk mitigation against a single hazard. While retrofit strategies to improve the seismic performance of reinforced concrete (RC) structures have been widely investigated, structural retrofitting against progressive collapse has received very little attention. Within this context, the present paper illustrates a numerical investigation on the influence of seismic retrofitting on structural robustness of a four-storey, five-bay, RC frame building designed only to gravity loads. Seismic performance and structural robustness were respectively evaluated in OpenSees through pushover and pushdown analyses of a fibre-based finite element model. Structural robustness was evaluated under two relevant column-removal scenarios, *i.e.*, the sudden loss of a central and a corner column, whereas earthquake resistance was assessed according to the N2 method, evidencing the need for seismic retrofitting. A retrofit measure based on carbon fibre reinforced polymers was then considered to avoid premature brittle failures. Analysis results show that this retrofit strategy was able to increase both seismic safety and structural robustness. Subsequently, a parametric analysis was carried out in order to evaluate the impact of beam span length and shear strength of the retrofitting system.

Keywords: Progressive collapse; robustness; seismic resistance; reinforced concrete buildings; structural retrofitting.

1. Introduction

Progressive collapse is a type of structural collapse that is triggered by heavy damage to a single or few structural components. That triggering event – which may be caused by an extreme loading condition – produces a chain of failures within the structural system, resulting into a disproportion between final and initial damage. Some iconic disasters, such as the collapse of the Ronan Point building (London, 1968) [1], the Murrah Federal Building (Oklahoma City, 1995) [2], and the World Trade Center (New York, 2001) [3], highlighted the huge consequences of progressive collapse in terms of loss of life and property, significantly increasing the interest of the research community, structural engineers, facility managers and stakeholders in this topic (*e.g.*, [4, 5]). Since the 1980s, and more significantly since 2001, many studies focused on various aspects of the problem through experimental testing (*e.g.*, [6–13]) and numerical simulation (*e.g.*, [14–21]), delineating design methods for progressive collapse resistance (*e.g.*, [22–24]). This created the basis for some guidelines and code provisions [25–27] that can be used in engineering practice to assess and reduce the potential of progressive collapse by means of structural and/or non-structural measures. In this context, there is a significant need for effective retrofit strategies able to improve the progressive collapse resistance of existing structures.

Another significant drawback of many existing constructions is related to their seismic vulnerability, as highlighted by several earthquakes worldwide (*e.g.*, [28, 29]). On the one hand, most of the existing structures were built according to past codes without modern design criteria, resulting in insufficient levels of seismic capacity; on the other, missing or inadequate maintenance of such constructions produces high levels of deterioration, further increasing their seismic vulnerability [30]. Nevertheless, in the last few decades, a large number of seismic retrofit strategies have been proposed and industrialised for their widespread implementation in practice (*e.g.*, [31–39]). Some researchers focused on reducing the seismic demand using base isolation systems or supplemental damping devices (*e.g.*, [31–34]), whereas other studies were aimed at increasing the seismic capacity (*e.g.*, [35–39]). Within this second category of vulnerability mitigation strategies, the use of fibre reinforced polymers (FRPs) for seismic strengthening of reinforced concrete (RC) beams and columns was evaluated in several studies (*e.g.*, [37–39]). Pampanin *et al.* [37] experimentally investigated the effectiveness of carbon

* Corresponding author.
Email address: fulvio.parisi@unina.it.

fibre reinforced polymer (CFRP) sheets through quasi-static cyclic tests on four beam-column sub-assemblies and a reduced-scale, three-storey, three-bay frame system. The results showed no damage in beam-column joints retrofitted with CFRPs allowing an appropriate global inelastic mechanism under cyclic loading. Pohoryles *et al.* [38] reviewed the state-of-the-art of FRP-based retrofitting strategies for beam-column joint sub-assemblies, evidencing how FRPs can be an important retrofit measure to address a number of deficiencies in non-seismically designed RC members framing into beam-column joints. Indeed, the application of FRPs can strongly improve the seismic behaviour of RC frame structures, avoiding damage concentration within beam-column joints that usually produces brittle failures and premature collapse.

In contrast to the extensive literature on seismic retrofitting, a very limited number of research studies focused on developing and investigating retrofit strategies to avoid the progressive collapse of structures. Regarding RC buildings, Li *et al.* [40] carried out an experimental study aimed at ensuring the sustainability of a structure prone to progressive collapse, using a rapid method for retrofitting RC frames with CFRP wraps. These researchers performed a progressive collapse test on a CFRP-retrofitted, 1/3 scale, RC frame with four bays and two storeys, showing that the selected retrofitting method can effectively and quickly restore the original capacity after progressive collapse. Jinkoo and Woo-Seung [41] numerically investigated the effect of prestressing tendons on the progressive collapse performance of a 6- and a 20-story RC structure subjected to a sudden column loss scenario, highlighting a stable behaviour in case of external prestressing tendons along beams. Based on nonlinear time-history analyses, Shayanfar *et al.* [42] demonstrated that the combined use of additional steel rebar and CFRP sheets on beams could be an efficient strategy for structural retrofit of RC frame buildings against progressive collapse. Similarly, Orton *et al.* [43] proposed and investigated a strategy to protect RC structures from progressive collapse by providing continuity of reinforcement in concrete beams through CFRPs. Experimental tests were carried out on seven beams underlining that the use of CFRP sheets allows reaching 60% and 108% of design load required by GSA guidelines [27], respectively, for positive and negative moments. Orton *et al.* [43] highlighted that, when beams do not have sufficient rotational ductility to develop catenary action, the continuity provided by the positive moment reinforcement may not significantly improve the progressive collapse resistance. In addition, CFRP sheets were also used to improve the flexural strength of the beams, requiring 4.5 times more CFRPs than those used to provide continuity of negative moment reinforcement. Qian *et al.* [43] experimentally investigated the use of externally bonded glass fibre–reinforced polymer (GFRP) sheets to mitigate the progressive collapse resistance of precast concrete buildings. Experimental tests were performed on three 1:3 scale multi-panel precast concrete sub-structures to evaluate the impact of detailing and strengthening solution on the progressive collapse resistance of structures with deficient detailing. Recently, Qin *et al.* [45] experimentally and numerically investigated the behaviour of beam-column sub-assemblages with steel-FRP composite bars (SFCBs). Three specimens with longitudinal SFCBs, ordinary steel bars and hybrid bars were compared to each other. The use of SFCBs showed higher performances with respect to the other solutions, allowing the development of flexural, compressive arch and catenary actions. Numerical simulations confirmed that the installation of SFCBs can be able to effectively reduce the progressive collapse vulnerability of RC frames.

The above-mentioned studies focused on structural retrofitting against single hazards. Nonetheless, as discussed by – among others – Li *et al.* [46], the likelihood of multiple hazards has sharply increased due to the rapid population growth and economic development. This leads to the importance of considering the interaction between different hazards in the design, assessment and retrofit of structures [47]. In this respect, the interaction between seismic and robustness designs is a matter of discussion because of the differences between the effects of earthquake ground motion and those of, for instance, the failure of a structural component. Nonetheless, the outcomes of several studies indicate some interesting chances to meet multiple performance objectives through the structure's ability to develop different behavioural modes depending on the type of actions it is subjected to.

Probabilistic simulations of European frame buildings based on incremental dynamic analysis (IDA) [16] and pushdown analysis (PDA) [48] of fibre-based finite element (FE) models showed a significant, positive impact of seismic design on robustness against single-column loss scenarios. That finding was consistent with previous investigations based on PDA of lumped plasticity FE models [15], which, however, remarked an insufficient robustness level under the simultaneous loss of multiple columns in line with IDA results [49]. Further studies were carried out to develop and validate solutions for the multi-hazard design of RC frame structures against earthquakes and progressive collapse. Feng *et al.* [50] investigated new RC frame structures, proposing a novel kinked rebar configuration for beams to simultaneously improve seismic resistance and robustness. The need to improve that design solution was already envisaged in the paper by Feng *et al.* [50] to eliminate drawbacks, such as the lower initial bending capacity of RC cross-sections with kinked rebar (compared to those reinforced with traditional, straight steel bars) and potential shear failure in case of kinked rebar located within the shear beam span.

Lin *et al.* [51, 52] outlined that considering seismic and progressive collapse designs individually may produce an undesirable performance of the structure as well as the waste of construction materials. Therefore, those researchers proposed and experimentally validated a novel design solution for precast RC frame structures based on beam-column connection through unbonded post-tensioning tendons, energy dissipating steel angles, and shear plates. The proposed design solution was able to provide the frame system with important capacity features, such as large rotational capacity of beams, slight damage, self-centring, and ease of repair.

Despite these research efforts, the influence of seismic retrofitting on the robustness of RC frame structures still needs to be investigated. This paper presents a numerical study on the impact that CFRP retrofitting of beams and columns may have on the structural robustness of low-rise RC frame buildings designed only to gravity loads according to Eurocode 2 [53]. The numerical investigation moved through the following steps: *(i)* structure-specific assessment of dynamic amplification factor (*DAF*) of gravity loads for subsequent progressive collapse analysis; *(ii)* robustness assessment of the structure based on PDA and offline shear safety checks under two major column-removal scenarios; *(iii)* seismic performance assessment through pushover analysis and local safety checks, *(iv)* design of CFRP seismic retrofitting and impact assessment on structural robustness and *(v)* parametric analysis able to highlight the parameters that can affect the progressive collapse resistance.

2. Description, modelling and DAF assessment of the case-study structure

2.1. Characteristics and modelling of the structure

This numerical study deals with a multi-storey RC frame building that was designed only to gravity loads in accordance with recommendations of Eurocode 2 [53]. Such a case-study structure was chosen among those analysed in previous studies [16, 48, 49, 54] because it is representative of low-rise, modern European RC buildings not designed for earthquake resistance. This allows general conclusions to be drawn according to numerical results, which is a key point for code development, implementation in engineering practice, and future research advances.

The structure has a rectangular shape in plan and consists of five storeys, five primary frames with six bays in the *x*-direction, and seven secondary frames with four bays in the *y*-direction. As illustrated in Figure 1a, a 2D framed system in the *x*-direction was extracted from the 3D structural model; this choice was motivated by the typical features of European constructions [15], according to which primary frames provide the main support to one-way joist slabs. In progressive collapse analysis, primary frames must carry most of the gravity loads through the activation of alternative load paths, governing the overall resistance of the building significantly more than secondary frames. The 2D frame is characterised by a span length of 5 m, reaching a total length of 30 m; the frame height is equal to 15 m, with an inter-storey height of 3 m.

Beams are characterised by a rectangular cross-section, 300×500 mm^2 in size, and a uniform longitudinal reinforcement consisting of 6 Ø18 steel bars (where Ø is the bar diameter). Columns have a squared cross-section, 400×400 mm^2 in size, and uniform longitudinal reinforcement consisting of 8 Ø18 steel bars. It is also noted that steel reinforcement is assumed to be made of ribbed bars rather than smooth bars, the latter being more representative of old RC frame buildings [15] that are not considered in this study. For both beams and columns, the transverse steel reinforcement is made of Ø8 stirrups with 200 mm spacing, whereas the concrete cover is set to 40 mm. Figures 1b and c also show the dimensions and reinforcement of cross-sections for both beams and columns. The influence of the infill walls was neglected in the structure modelling. Nonetheless, previous studies [56–58] pointed out that non-structural components may have a significant impact on the structural response to extreme loads (*e.g.*, seismic shaking, impact, blast), but this is beyond the objectives of the current study and will be investigated in future works.

Structural modelling and nonlinear analyses for both seismic and progressive collapse assessments were carried out through OpenSees [55], which was experimentally validated for progressive collapse analysis in previous studies (*e.g.*, [48]). Nonlinear capacity modelling of the structure was based on a spread plasticity FE approach with displacement-based fibre formulation. Each cross-section was discretised in 120 fibres, specifically 100 fibres relating to the confined concrete and 20 fibres for the remaining part, as illustrated in Figures 2a and b. A direct integration of individual fibres' uniaxial material response was used to simulate the diffusion of inelasticity over cross-sections and member length, allowing the assessment of sectional stresses and strains during the incremental loading process. A mesh sensitivity analysis was carried out by assuming both smaller and larger numbers of fibres. Nonetheless, the selected discretisation of cross-sections into

120 fibres was able to provide reliable results, ensuring a very good trade-off between computational accuracy and cost.

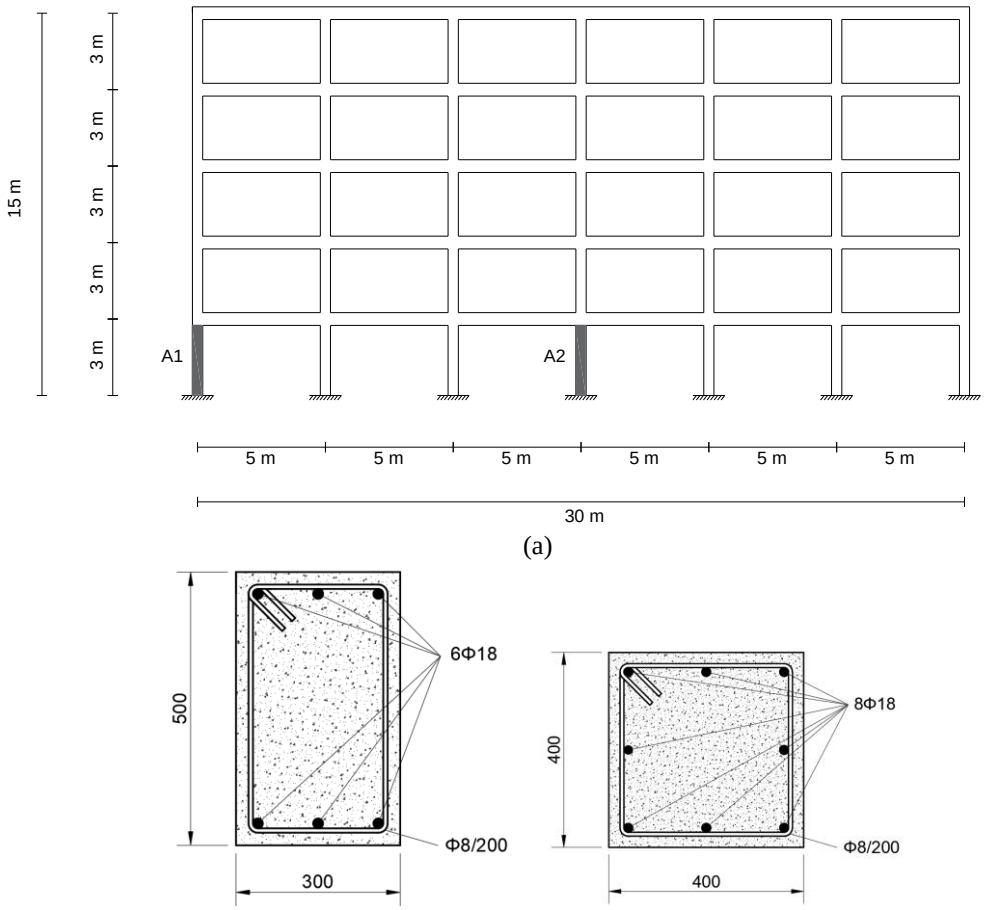

Figure 1. Case-study structure: (a) elevation view with identification of column removal scenarios at the ground floor; cross-sections and reinforcement arrangements in (b) beams and (c) columns (dimensions in mm).

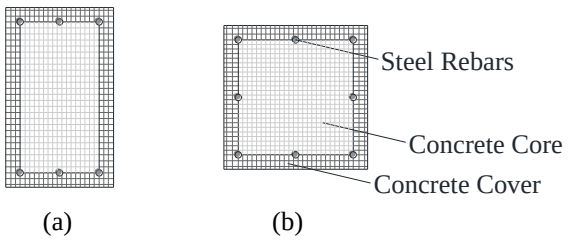

Figure 2. Fibre discretization of RC cross section: (a) beams; (b) columns.

The RC frame is made of C20/25 concrete and B450C steel reinforcement bars, which are common materials used for RC buildings. Mechanical properties of concrete and steel are outlined in Table 1, whereas the weight per unit volume was set to 25 kN/m^3. The uniaxial Kent-Scott-Park constitutive model [59] (*i.e.*, 'Concrete01' in OpenSees) was adopted to simulate the stress–strain behaviour of confined concrete within core of RC cross-sections. That stress–strain relationship is characterised by three branches as follows (see Figure 3a): a nonlinear rising branch up to peak compressive strength f'_{cc} and axial strain ε_{cc0}; a linear descending branch up to residual compressive strength f'_{ccu} and axial strain ε_{ccu}; a residual strength plateau with unlimited strain. Assuming a characteristic compressive strength of unconfined concrete f_{ck} = 20 MPa, the mean compressive strength was set to $f_{cm} = f_{ck} + 8$ according to Eurocode 2 [53]. In case of concrete cover, the lack of concrete confinement was assumed, and so, the peak compressive strength was assumed to be $f'_c = f_{cm} < f'_{cc}$,

with $\varepsilon_{cu} < \varepsilon_{ccu}$ and zero residual strength. A uniaxial bilinear model (see Figure 3b) with kinematic hardening, which is defined through Young's modulus E_0, yield strength f_y, and hardening ratio k, was adopted for reinforcing steel (*i.e.*, 'Steel01' in OpenSees).

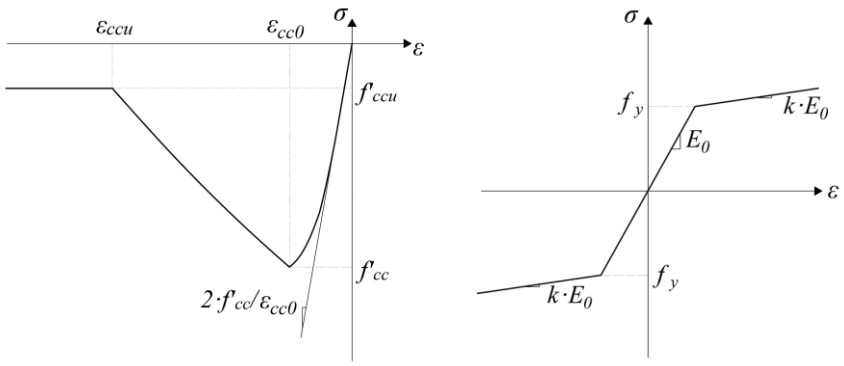

(a) (b)

Figure 3. Uniaxial stress–strain models: (a) Kent-Scott-Park model for concrete; (b) bilinear model for steel.

Table 1. Mechanical properties of concrete and steel.

Material	Structural member	f_y [MPa]	E_0 [GPa]	k	f'_{cc} [MPa]	f'_{ccu} [MPa]	E_c [GPa]	ε_{cc}	ε_{ccu}	ε_{cu}
Concrete	Beam (core)	–	–	–	29.41	5.88	24.87	$2.36\cdot10^{-3}$	$8.01\cdot10^{-3}$	–
	Column (core)	–	–	–	29.14	5.82	24.87	$2.34\cdot10^{-3}$	$6.90\cdot10^{-3}$	–
	Any (cover)	–	–	–	28.00	5.60	23.50	$2.38\cdot10^{-3}$	–	$3.50\cdot10^{-3}$
Steel	Any	450	200	0.01	–	–	–	–	–	–

Geometric nonlinearities in the form of both large displacements/rotations and P-Delta effects were considered by means of a total corotational transformation, which was validated in previous studies (*e.g.*, [48]).

Dead and live loads were applied as concentrated loads according to the discretisation of each structural member into five model elements, as shown in Figure 4. A parametric study showed that a further increase in the number of model elements would not significantly increase computational accuracy. Beam-column joints were modelled as rigid elements as done in several previous research studies (*e.g.*, [15, 16, 54]). Figure 4 shows the frame layout, together with the identification numbers and labels for beams, columns, and beam-column joints.

The case study structure was already investigated by Parisi *et al.* [54] through FE models developed in SeismoStruct [60]. A comparison between SeismoStruct and OpenSees has been already performed in literature [61]. Also in that case, the FE model was developed according to a spread plasticity approach and rigid beam-column joints, considering geometric nonlinearities by means of a total corotational transformation. Therefore, the model used in this study was compared to that developed in SeismoStruct, revealing a good agreement in terms of modal properties (*i.e.*, vibration periods and mode shapes as well as corresponding participating mass ratios). Dynamic analysis was performed under the following design gravity load as per UFC guidelines [25]:

$$Q_d = 1.2DL + 0.5LL \tag{1}$$

where DL = 3 kN/m^2 and LL = 2 kN/m^2 represent dead and live loads, respectively. These values were equal to those used in [54].

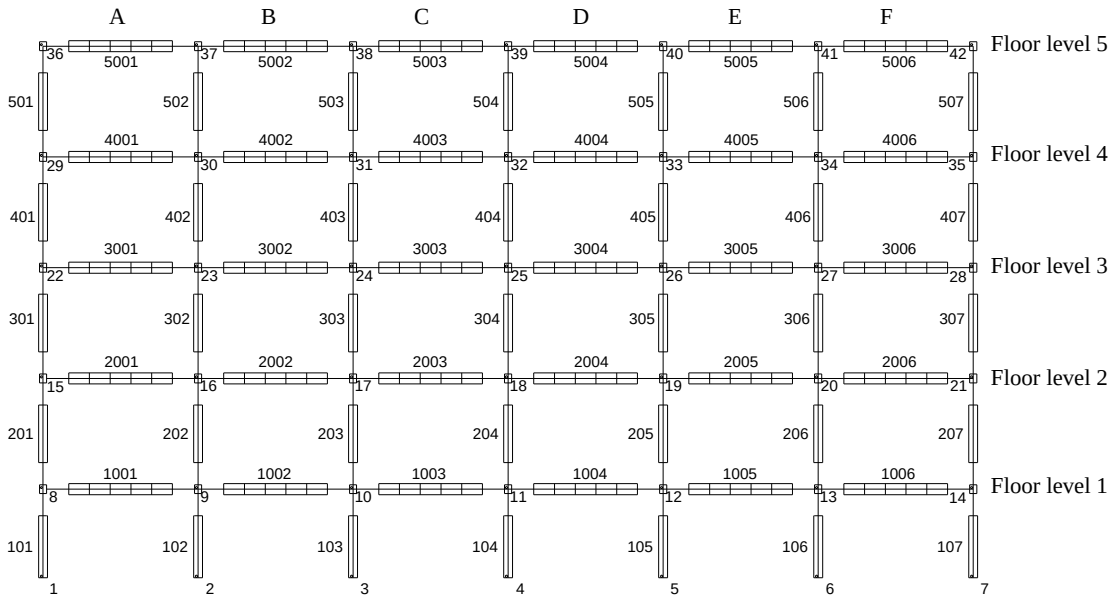

Figure 4. Elements' discretisation and designation of joints, floor levels, and vertical beam/column series.

2.2. Structure-specific assessment of dynamic amplification factor

The progressive collapse resistance and robustness of RC frame buildings can be evaluated by means of PDA, provided that design gravity loads on beams/floor areas above the removed column(s) are amplified through a dynamic amplification factor (*DAF*). Such a factor allows implicit consideration of vertical inertia forces that are generated in the portion of the structure involved in the progressive collapse. Nonetheless, there are no specific equations for *DAF* prediction in case of European frame buildings complying with Eurocodes. Dealing with case-study structures designed according to American codes, Table 3-5 of UFC guidelines [25] provides the following equation for nonlinear static analysis of RC frame structures:

$$DAF = 1.04 + \frac{0.45}{\frac{\theta_{pra}}{\theta_y} + 0.48} \tag{2}$$

where: θ_{pra} is the plastic rotation associated with a prescribed performance level; θ_y is the yield rotation of beams. It is noted that *DAF* is denoted as Ω_N in UFC guidelines. If θ_{pra} is set to 0.03 according to Table 4-1 of UFC guidelines and θ_y is calculated based on recommendations of Eurocode 8 [62], the *DAF* turns out to be 1.16. Nevertheless, in this study, the *DAF* was specifically assessed for the case-study structure by comparing the gravity load capacity resulting from PDA to that predicted via IDA in a previous study [54] under increasing vertical deformation induced by the sudden removal of a ground-floor column. Indeed, vertical deformation described in terms of beam drift θ was a common variable of PDA and IDA, which can be associated with a load multiplier (or factor) α defined by Parisi and Augenti [15] as follows:

$$\alpha = \frac{\sum_i R_i}{\sum_i R_i\left(Q_d\right)} \tag{3}$$

where: the numerator is the sum of vertical reaction forces R_i of base restraints during progressive collapse analysis (either PDA or IDA), which measure the gravity load capacity of the structure; the denominator is the sum of vertical reaction forces of base restraints $R_i(Q_b)$ corresponding to the design gravity loads, which measure the vertical resistance demand on the structure associated with Eq. (1). According to Eq. (3), both PDA and IDA curves plotted in the Q_b–θ plane can be transformed into the α–θ plane, thus resulting in dimensionless capacity curves. Such a transformation is particularly useful

because the maximum load multiplier α_{max} allows a direct verification of structural robustness. Indeed, $\alpha_{max} \geq 1$ indicates a sufficient structural robustness to the column-removal scenario under consideration. From a graphical standpoint, this also means that the performance objective of structural robustness is met if the α–θ curves corresponding to the selected scenarios reach or exceed the horizontal threshold line associated with $\alpha = 1$.

Regardless of the analysis type, the vertical drift θ was defined as follows:

$$\theta = \tan^{-1}\left(\frac{D_v}{L_b}\right) \tag{4}$$

where D_v represents the vertical displacement of the control point, which was assumed to be the upper joint of the removed column; L_b is the beam length, which is equal to 5 m.

According to Figure 1a, progressive collapse analysis was run under two notional damage scenarios denoted as A1 and A2, which respectively simulate the sudden loss of corner and central columns at the ground floor of the case-study structure. Figures 5a and b compare the results of the PDAs performed in this study to those derived by Parisi *et al.* [54] through IDA. As expected, PDA with uniform gravity loads complying with Eq. (1) led to an overestimation of the gravity load capacity, as dynamic load amplification on beams above the removed column was not considered. Circles and squares in Figure 5 indicate the points of peak load capacity in PDA and IDA, respectively.

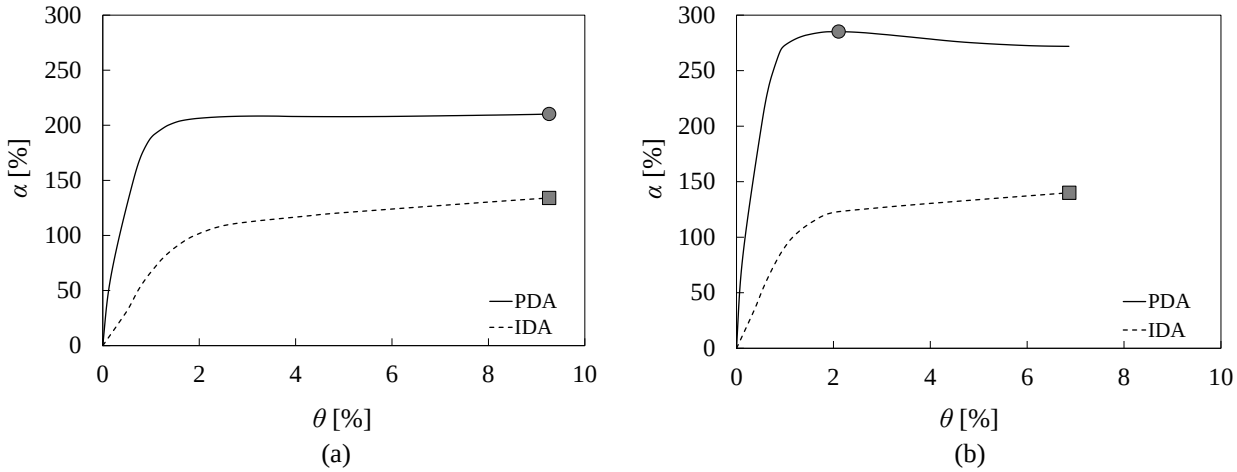

Figure 5. Comparison between pushdown analysis (PDA) and incremental dynamic analysis (IDA) in terms of dimensionless capacity curves: (a) scenario A1; (b) scenario A2.

Therefore, *DAF* was specifically quantified for the case-study structure as follows:

$$DAF = \frac{\alpha_{PDA}}{\alpha_{IDA}} \tag{5}$$

where α_{PDA} and α_{IDA} are the load multipliers computed through PDA and IDA, respectively, under varying θ. Figure 6 shows *DAF*–θ curves for both column-removal scenarios, evidencing a realistic estimation of dynamic load amplification for the Eurocode-conforming structure under study. Indeed, *DAF* is always higher than unity up to large vertical drifts. It is also underlined that the *DAF*-value predicted through Eq. (2) according to UFC guidelines [25] (*i.e.*, *DAF* = 1.16 corresponding to $\theta = 0.03$) is significantly lower than that directly computed through PDA-IDA comparison. This further remarks the need for additional and comprehensive studies aimed at the *DAF* evaluation for building structures designed in accordance with the Eurocodes, particularly to Eurocode 2 [53] and Eurocode 8 [62] for gravity-load designed and earthquake-resistant structures, respectively.

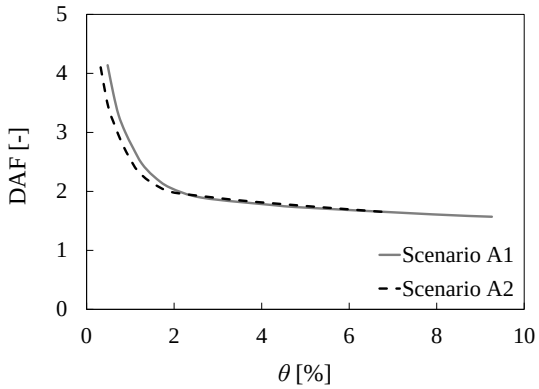

Figure 6. Evaluation of dynamic amplification factor (*DAF*) for the case-study structure and each scenario.

3. Progressive collapse capacity assessment

The *DAF* was specifically evaluated for the case-study structure, and progressive collapse analyses were carried out to assess structural robustness. The progressive collapse capacity of the structure was evaluated through PDA with displacement control, separately for each of the two relevant column-removal scenarios labelled as A1 and A2 in Figure 1a. Those scenarios were selected as they were previously found to be the worst cases of column loss for the structure under investigation [54]. It is noteworthy that, in previous studies by some of the authors of this paper [16, 48, 54], the 2D frame was supposed to be located on the building perimeter, whereas the structural system is herein supposed to be an internal primary frame. Such an assumption provides a maximisation of dead and live loads transmitted from floors to beams, resulting in a design gravity load on beams equal to Q_{bd} = 23 kN/m according to the load per unit floor area defined through Eq. (1). The load Q_{bd} on beams above the removed column was then amplified through the *DAF*-value computed through the curves in Figure 6.

In this study, the progressive collapse assessment is carried out according to a threat-independent approach, where the structure is analysed under notional removal of structural components (*i.e.,* a single column in this case) in line with the alternate load path (ALP) method [25, 27]. In this respect, the consideration of an internal primary frame rather than its twin system located on the building perimeter does not affect the selection of column-removal scenarios at the ground floor. Conversely, this should be taken into account into threat-dependent ALP simulations for progressive collapse risk assessment [5], where initial internal damage to columns may have a significantly lower probability of occurrence in the case of residential buildings. This issue is, however, out of the scope of this study.

3.1. Pushdown capacity curves and resisting mechanisms of beams

The progressive collapse resistance of the selected frame was evaluated under the same scenarios considered in previous sections, namely, the notional removal of the corner column (scenario A1) and central column (scenario A2), separately. Figure 7 shows the dimensionless pushdown capacity curves, which indicate reduced levels of structural robustness compared to those derived for the perimeter frame (Fig. 5). In the case of corner column removal, the maximum load multiplier (*i.e.,* α_{max}) reduced from 181% to 99%, evidencing an insufficient level of robustness to design gravity loads. In the case of internal column removal, the progressive collapse capacity was reduced by 92%, even though α_{max} was still found to be higher than unity. The dashed line in Figure 7 indicates a significant global effect of catenary action from beams, which allows a further increase in the maximum load multiplier at large drifts. This was further investigated in terms of axial forces in beams, as discussed below.

PDA was carried out without any limitation to the ultimate steel strain, according to the bilinear constitutive model presented in Section 2.1. Therefore, the attainment of several strain thresholds in longitudinal steel bars of beams was investigated to assess the impact of different values of ultimate steel strain on progressive collapse capacity assessment. As discussed in previous studies (*e.g.,* [54]), the ultimate elongation of modern (ribbed) steel bars in design and assessment of RC frame structures is typically set to ε_{su} = 4%, ensuring the assumption of plane sections after flexural deformation in Euler-Bernoulli beam models. Although that value of ultimate steel strain does not affect nonlinear response analysis under, for instance, seismic actions, the assumption of a realistic value for ε_{su} becomes of paramount importance in progressive

collapse analysis. Indeed, higher values of ultimate steel strain allow RC beams to develop first compressive arch action (CAA) and afterwards tensile catenary action (TCA) under increasing vertical displacement at the location of the removed column(s). CAA and – most importantly – TCA are large-displacement resisting mechanisms that can strongly support or even be the most significant source of a structure's survivability under extreme loading conditions. Hence, the authors monitored the attainment of three values of ultimate steel strain, *i.e.*, 4%, 10%, and 20%, the latter being very close to fracture steel strain of longitudinal bars that is associated with actual collapse of RC frames under the column loss scenario [5]. Figure 8 shows the identification of vertical drift levels corresponding to the selected values of ultimate steel strain for both column-removal scenarios. The residual part of capacity curves after the attainment of each strain threshold is plotted in different colours to highlight how much ε_{su} influences the final judgement on structural robustness in terms of peak load capacity (measured through α_{max}) and maximum vertical drift (*i.e.*, θ_{max}). Previous experimental and numerical studies indicated that progressive collapse of RC frames is actually related to an ultimate drift θ_u ranging between 15% and 20% [5, 63]. Figures 8a and b clearly show that assuming ε_{su} = 4% produces essentially the same maximum drifts regardless of the selected scenario, resulting in $\theta_{max} << \theta_u$. If ε_{su} is set to 10% or 20%, the beams can develop both CAA and TCA, allowing the RC frame to reach θ_{max} = 18% and $\theta_{max} = \theta_u$, respectively.

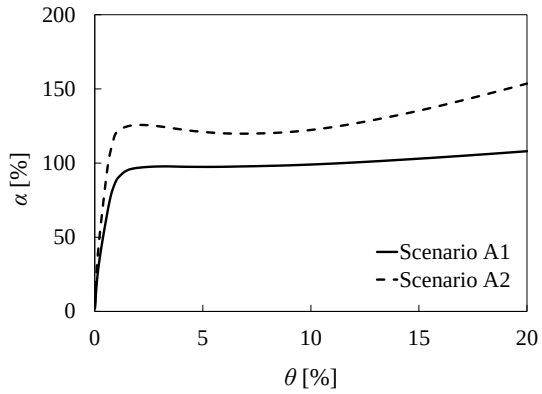

Figure 7. Dimensionless pushdown capacity curves of the internal primary frame.

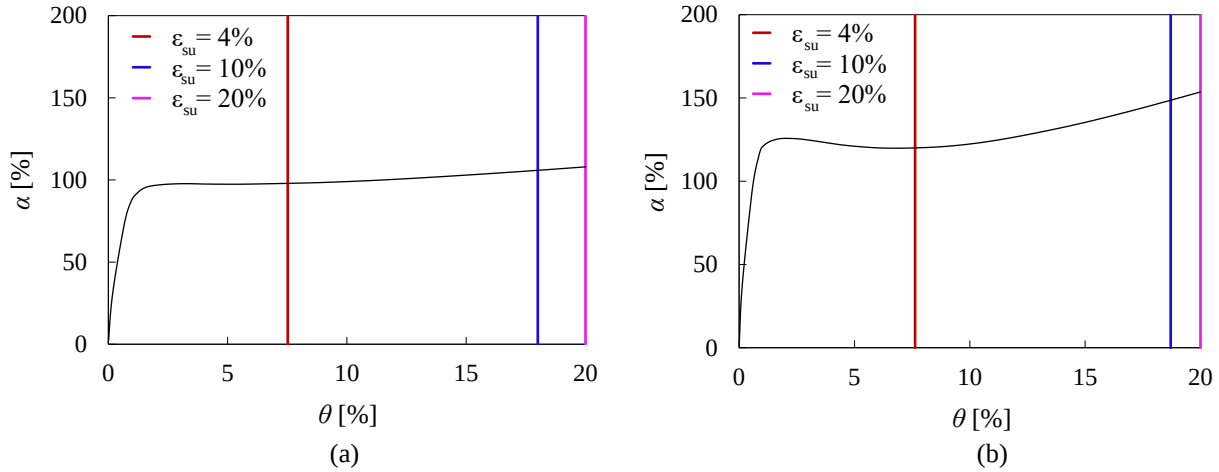

Figure 8. Influence of ultimate steel strain on pushdown capacity curves: (a) scenario A1; (b) scenario A2.

More specifically, CAA and TCA allow an increase in α at drifts larger than approximately 7%, resulting in a sort of global hardening behaviour, especially in scenario A2. This is in agreement with axial forces in beams (denoted as *N*) under varying drift, which are plotted in Figure 9b for scenario A1 and Figure10b for scenario A2 together with near-collapse deformed shapes in Figures 9a and 10a. As expected, the beams above the removed column at floor levels 1 and 5 experienced the largest variations in axial force, according to the largest variations in shear forces within columns at the same floor levels.

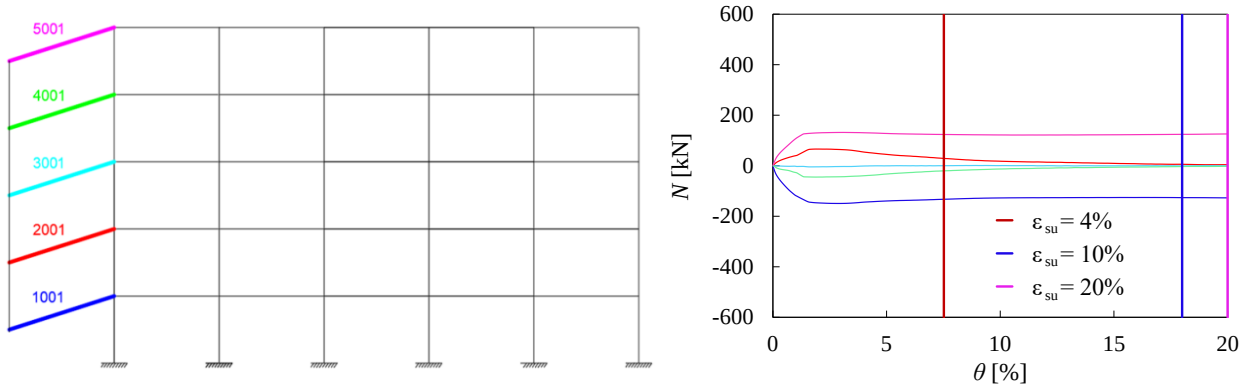

(a) (b)

Figure 9. Beam behaviour under scenario A1: (a) beams labelling; (b) axial force under varying drift and ultimate steel strain.

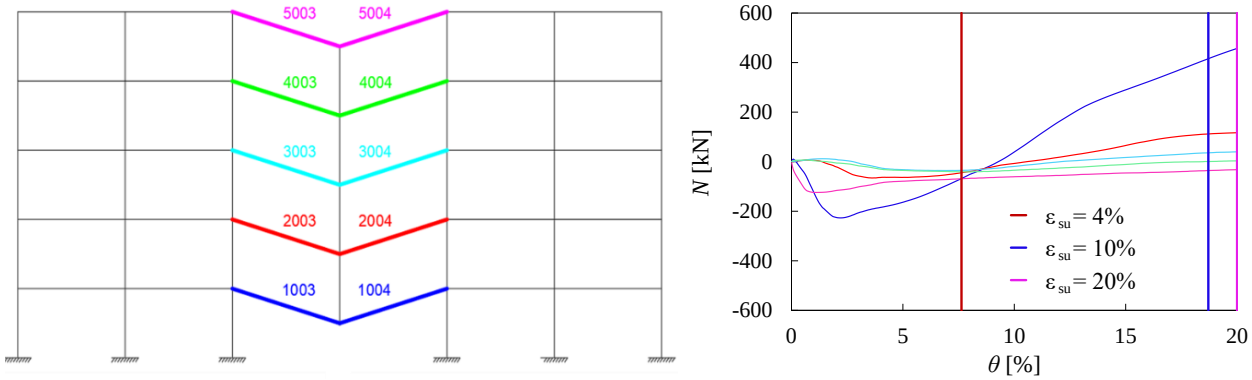

(a) (b)

Figure 10. Beam behaviour under scenario A2: (a) beams labelling; (b) axial force under varying drift and ultimate steel strain.

Nonetheless, scenario A2 is the most interesting analysis case because the beams at floor levels 1 and 5 were first subjected to compressive axial loading (arch action) up to a vertical drift $\theta_{max} \approx 8\%$ (corresponding to a maximum steel strain $\varepsilon_{s,max}$ slightly larger than 4%) and then to tensile axial loading (catenary action) till collapse. TCA was thus mobilised when maximum axial strain in longitudinal steel bars exceeded 4%, gradually reaching 10% and 20%. Axial forces in beams at other floor levels gradually vanish under increasing drift. The development of catenary action was maximised in beams at floor level 1, namely, those labelled as 1003 and 1004 in Figure 10a, as highlighted by blue curves in Figure 10b. This means that the catenary action in each beam is not only a function of the amount, ultimate elongation and anchorage of longitudinal steel reinforcement, as it also depends on the relative location of the beam with respect to the removed column.

3.2. Shear safety checks

Given that the structure was designed only to gravity loads according to Eurocode 2 [53] with no particular care about strength hierarchy, shear failure in beams and columns may occur and affect the progressive collapse capacity according to previous studies on RC frame buildings not designed for earthquake resistance (*e.g.*, [15]). Shear failure mechanisms were not modelled in the FE model implemented in OpenSees [55], so offline shear safety checks were carried out on the structure to identify the analysis step related to the first occurrence of shear failure. To that aim, the capacity model proposed by Biskinis and Fardis [64] – which is currently included in Eurocode 8 [62] – was used to evaluate the shear resisting force of frame members through the following equation:

$$V_{Rd} = V_N + V_c + V_w \quad (6)$$

where V_N, V_c and V_w denote the contributions to shear strength from the axial load (in the form of an inclined internal strut resisting mechanism), the concrete, and the transverse reinforcement (according to the Ritter-Mörsch truss resisting mechanism analogy) respectively. For the sake of brevity, readers can find details on the computation of Eq. (6) in [62] and [64].

Following a step-by-step evaluation of shear demand on frame members during the PDA, the demand-to-capacity ratios (DCRs) listed in Tables 2 and 3 were obtained. In Table 2, DCRs on the same line are associated with different beam spans, which are labelled in alphabetical order from the left- to the right-hand side (*i.e.*, from A to F, according to Figure 4). DCRs belonging to the same column of Table 2 are related to different floor levels. In case of corner column removal (scenario A1), post-processing of PDA results highlighted the first occurrence of shear failure in beam spans A, indicating a premature failure in the third step of progressive collapse analysis with DCR ranging from 1.01 (floor level 5) to 1.49 (floor level 1) as shown in Figure 12a.

Table 2. Demand-to-capacity ratios corresponding to the first occurrence of shear failure in beams*.

Floor level	Beam span											
	Scenario A1						Scenario A2					
	A	B	C	D	E	F	A	B	C	D	E	F
1	**1.49**	0.74	0.59	0.60	0.60	0.63	0.54	0.56	**1.44**	**1.44**	0.56	0.54
2	**1.15**	0.55	0.50	0.49	0.49	0.50	0.52	0.56	**1.42**	**1.42**	0.56	0.52
3	**1.15**	0.52	0.49	0.49	0.49	0.50	0.51	0.55	**1.40**	**1.40**	0.55	0.51
4	**1.16**	0.53	0.51	0.50	0.50	0.49	0.52	0.53	**1.40**	**1.40**	0.53	0.52
5	**1.01**	0.54	0.44	0.44	0.44	0.47	0.55	0.66	**1.39**	**1.39**	0.66	0.55

* Bold figures indicate DCRs > 1, *i.e.*, failed elements.

Table 3. Demand-to-capacity ratios corresponding to the first occurrence of shear failure in columns.

Floor level	Column line													
	Scenario A1							Scenario A2						
	1	2	3	4	5	6	7	1	2	3	4	5	6	7
1	0.00	0.22	0.07	0.06	0.08	0.09	0.01	0.24	0.13	0.32	0.00	0.32	0.13	0.24
2	0.89	0.31	0.32	0.26	0.25	0.24	0.02	0.16	0.05	0.46	0.00	0.46	0.05	0.16
3	0.57	0.41	0.24	0.23	0.24	0.24	0.00	0.19	0.01	0.50	0.00	0.50	0.01	0.19
4	0.58	0.43	0.23	0.25	0.25	0.25	0.01	0.20	0.05	0.54	0.00	0.54	0.05	0.20
5	0.79	0.59	0.41	0.35	0.33	0.32	0.03	0.25	0.13	0.84	0.00	0.84	0.13	0.25

By contrast, the notional loss of the central column (scenario A2) led to the first occurrence of shear failure in beams belonging to spans C and D (see Figure 12b), showing DCR between 1.39 and 1.44. It is worth noting that other beams were subjected to significantly lower levels of shear demand. Table 3 shows that shear failure did not occur in columns.

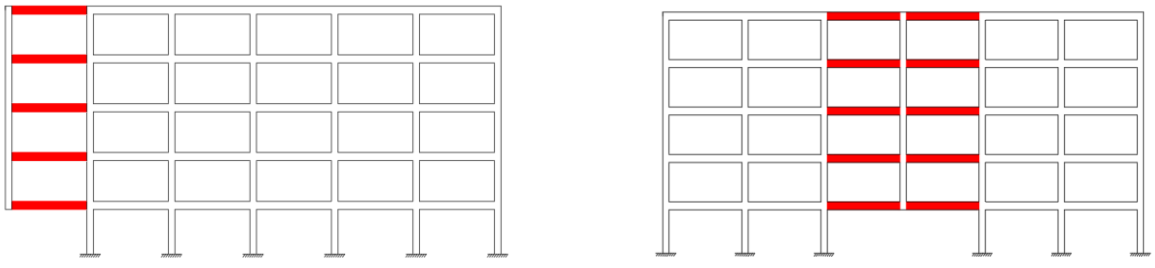

(a) (b)

Figure 12. Location of shear failures: (a) scenario A1; (b) scenario A2.

The first occurrence of shear failure is also marked by red circles on dimensionless capacity curves depicted in Figures 13a and b, which are respectively related to scenarios A1 and A2. Those curves show that shear failure in beams occurred

at load levels that were lower or approximately equal to 50% of design gravity load. Therefore, the level of structural robustness for the case-study structure is significantly influenced by shear failure, highlighting the need for retrofitting to mitigate the progressive collapse potential.

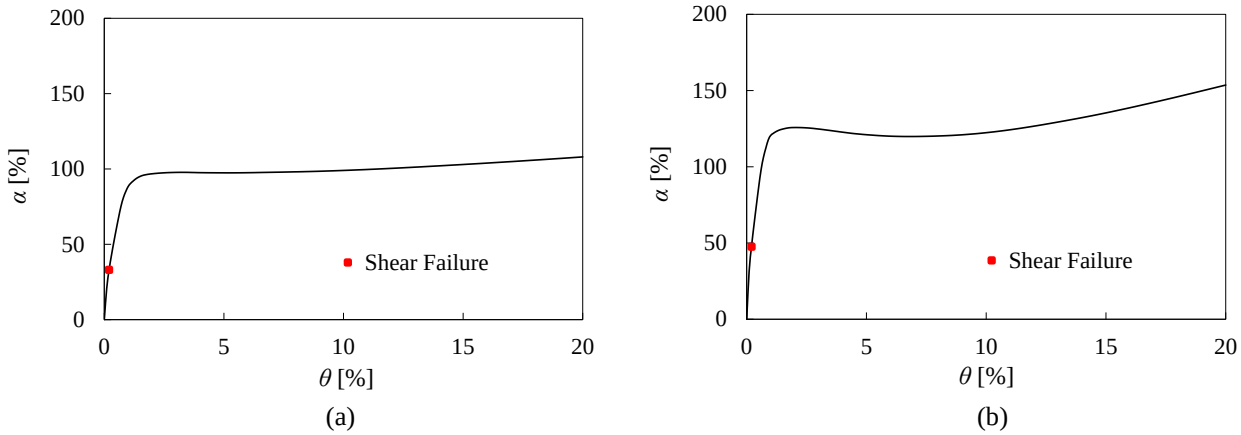

Figure 13. Identification of first shear failure on dimensionless capacity curves: (a) scenario A1; (b) scenario A2.

4. Seismic performance assessment

In the second part of this study, a seismic assessment of the structure was carried out by means of nonlinear incremental static (pushover) analysis, according to Eurocode 8 – Part 3 [62]. The building was assumed to be located in L'Aquila, Italy, which falls within a high-seismicity area and was severely damaged by a M6.3 earthquake in 2009 [28]. Seismic hazard parameters were defined to assess the design action, and the structure was seismically assessed through global and local checks.

4.1. Seismic action modelling and global safety checks

A site-dependent seismic hazard assessment was carried out according to the Italian building code NTC2018 [65]. Given that the case-study structure belongs to a residential building, a nominal lifetime V_N = 50 years and an occupancy factor C_U = 1 (corresponding to occupancy class II) were assumed, resulting in a reference (temporal) period for seismic assessment $V_R = V_N C_U$ = 50 years. Site-dependent hazard maps adopted by the NTC2018 define seismic hazard through the following parameters: the horizontal peak ground acceleration on type A ground (*i.e.*, rock or rock-like geological formation) with horizontal topographic surface (topographic category T1), a_g; the maximum amplification factor of horizontal spectral acceleration, F_o; and upper bound period of the constant spectral acceleration branch on type A ground, T_C^*. The seismic assessment was performed for life safety limit state, so seismic hazard parameters were evaluated by assuming a probability of exceedance in the reference period P_{V_R} = 10%. According to the NTC2018's assumption of homogeneous Poisson's stochastic process for earthquake occurrence [65], a return period of design earthquake T_R = 475 years was considered, resulting in the following values of seismic hazard parameters: a_g = 0.26*g*; F_o = 2.36, which is lower than the value recommended by Eurocode 8 – Part 1 [66] (*i.e.*, F_o = 2.5) because that European code does not account for the influence of deep geology on seismic hazard); and T_C^* = 0.350 s. Site amplification of earthquake ground motion was taken into account by assuming peak ground acceleration $PGA = a_g S$, where S is a soil factor derived as a stratigraphic amplification factor (S_S) times a topographic amplification factor (S_T). The case-study structure was supposed to be located on type B ground with a horizontal topographic surface, resulting in S_S = 1.154, S_T = 1, and hence PGA = 0.3*g*. Opposed to Eurocode 8 – Part 1 [66], the NTC2018 [65] accounts for stratigraphic conditions also in the definition of the upper bound period T_C for flexible soil types (*i.e.*, ground types different from A), then providing site-dependent elastic response spectra that approximate fairly well uniform hazard spectra. Assuming a type B ground, a soil factor C_C = 1.357 was computed according to NTC2018 [65], resulting in $T_C = C_C T_C^* = 0.475\,\text{s}$. Based on T_C, the lower bound period of the constant spectral acceleration branch was found to be $T_C = T_C / 3 = 0.158\,\text{s}$, whereas the lower bound period of the constant displacement branch was set to $T_D = 4a_g / g + 1.6 = 2.640\,\text{s}$. Such data allowed the definition of the elastic response spectrum for

subsequent seismic demand analysis.

Seismic capacity was evaluated by means pushover analysis, which was carried out with displacement control under the following load patterns: *(i)* a mode profile, which consists of lateral forces proportional to inertia masses times first mode displacements; and *(ii)* a mass profile, where lateral forces are proportional to inertia masses, assuming a uniform acceleration pattern along with the height of the structure. A beam-column joint at the roof level was selected as the control point for nonlinear static analysis. For each load pattern, the output of pushover analysis was a capacity curve, which was first scaled down according to the first-mode participating factor and then approximated through a bilinear diagram according to Eurocode 8 – Part 3 [66].

Seismic capacity and demand were then transformed in the acceleration-displacement plane, resulting in capacity and demand spectra, respectively. The seismic assessment was performed by comparing the inelastic displacement demand S_{di} to the displacement capacity d_u^*. The intersection between the demand and capacity spectra defined the performance point (PP), allowing the seismic safety assessment in terms of displacement DCR. The outcome of seismic performance assessment is shown in Figure 14, where: S_a and S_d are the spectral accelerations and displacements, respectively; S_{ay} is the yield spectral acceleration of the structure; and S_{de} is the elastic displacement demand (corresponding to point D and elastic acceleration demand S_{ae}). The displacement capacity and yield spectral acceleration define the capacity point C in Figure 14. Seismic performance assessment under mode and mass force profiles outlined DCR equal to 33% and 43%, respectively, indicating a satisfactory global performance of the structure.

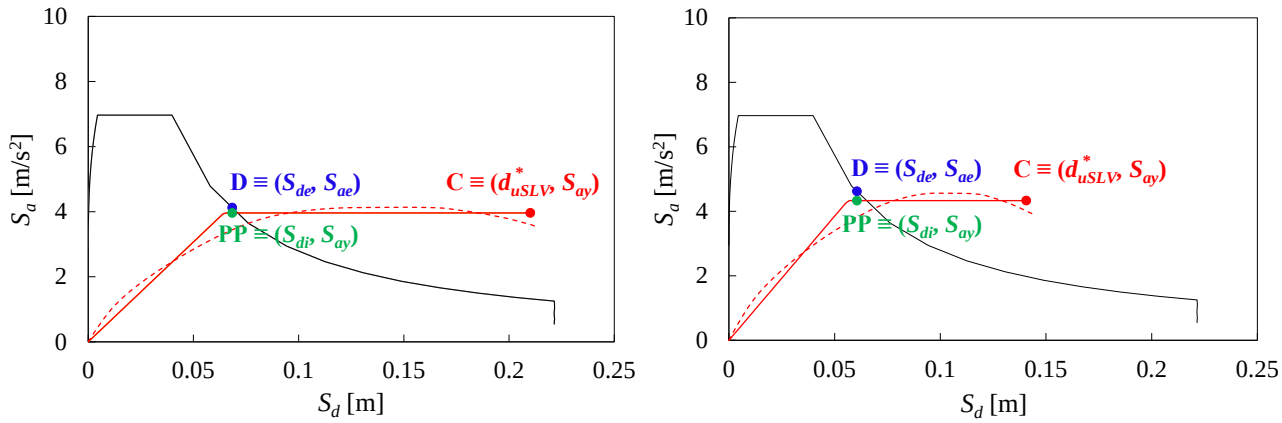

Figure 14. Global seismic performance assessment of case-study structure: (a) mode force profile; (b) mass force profile (blue, red, and green circles indicate the elastic demand, capacity, and performance points, respectively).

4.2. Local safety checks

Post-earthquake damage assessments have shown that gravity-load designed RC frame buildings often suffer brittle shear failures in beams and columns (*e.g.*, [28, 29]). Such failures can partially or totally neutralise the structure's global performance, so seismic safety of the case-study structure was locally assessed against those failure modes as made in previous progressive collapse analysis. Shear safety checks for beams and columns were carried out via the same capacity model used in Section 3.2 [64]. According to Eurocode 8 – Part 3 [66] and NTC2018 [65], those local checks were performed at the global performance point (green circle) identified in Figure 14. That modus operandi was thus different from that used in progressive collapse assessment, where local safety checks were carried out step by step to identify the first occurrence of shear failure. As a result, local checks for seismic assessment do not indicate the first occurrence nor the sequence of shear failures throughout the analysis because demand-to-capacity ratios are directly associated with displacement demand on the structure. Shear strength DCRs evaluated for beams and columns are listed in Tables 4 and 5, respectively, evidencing that most of those frame members were expected to fail in shear under the design earthquake. DCRs are complemented by the graphical identification of unsafe members shown in Figure 15, which agrees with structural symmetry in elevation.

Table 4. Beams shear checks: demand-to-capacity ratios corresponding to each force profile*.

Floor level	Beam span											
	Mass profile						Mode profile					
	A	B	C	D	E	F	A	B	C	D	E	F
1	**2.36**	**2.24**	**2.25**	**2.25**	**2.24**	**2.28**	**2.24**	**2.18**	**2.21**	**2.23**	**2.25**	**2.28**
2	**2.20**	**2.06**	**2.02**	**1.97**	**1.92**	**1.89**	**2.32**	**2.18**	**2.14**	**2.10**	**2.06**	**2.03**
3	**1.82**	**1.70**	**1.66**	**1.61**	**1.56**	**1.53**	**2.05**	**1.90**	**1.85**	**1.80**	**1.74**	**1.72**
4	**1.36**	**1.33**	**1.29**	**1.26**	**1.23**	**1.19**	**1.58**	**1.51**	**1.46**	**1.42**	**1.37**	**1.32**
5	**1.36**	**1.33**	**1.29**	**1.26**	**1.23**	**1.19**	**1.13**	**1.01**	**1.00**	0.98	0.98	0.89

* Bold figures indicate DCR > 1.

Table 5. Columns shear checks: demand-to-capacity ratios corresponding to each force profile*.

Floor level	Column line													
	Mass profile							Mode profile						
	1	2	3	4	5	6	7	1	2	3	4	5	6	7
1	**2.03**	**2.07**	**2.14**	**2.19**	**2.25**	**2.32**	**2.04**	**1.59**	**1.81**	**1.93**	**2.03**	**2.12**	**2.21**	**1.89**
2	**1.60**	**2.20**	**2.14**	**2.09**	**2.04**	**1.98**	**0.90**	**1.80**	**2.25**	**2.24**	**2.20**	**2.16**	**2.12**	**0.98**
3	**1.15**	**1.86**	**1.77**	**1.68**	**1.58**	**1.48**	**1.02**	**1.46**	**2.16**	**2.07**	**1.98**	**1.88**	**1.78**	**1.17**
4	0.70	**1.39**	**1.32**	**1.25**	**1.19**	**1.13**	0.74	**1.04**	**1.76**	**1.67**	**1.58**	**1.50**	**1.42**	0.91
5	0.02	0.81	0.79	0.75	0.71	0.63	0.60	0.18	**1.12**	**1.05**	0.99	0.93	0.81	0.65

* Bold figures indicate DCR > 1.

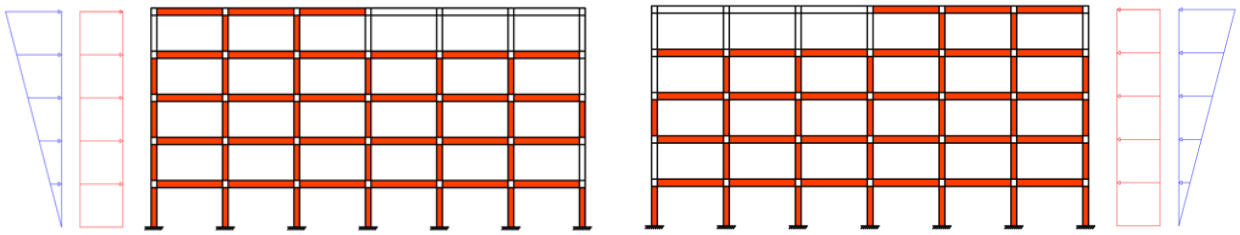

Figure 15. Identification of beams and columns failing in shear for each orientation of lateral forces.

5. Evaluation of progressive collapse resistance after structural retrofit intervention

5.1. Influence of seismic retrofitting on progressive collapse capacity

Following the analysis carried out in the previous sections, the safety of the case-study structure is undermined by the potential occurrence of local failures, which do not allow the structure to develop its global response. It should be noted that a seismic safety requirement of a gravity-load designed structure can be motivated by several instances, such as the updating of seismic hazard maps within a region or country, as frequently observed after past earthquakes and engineering seismology studies in Italy and other Euro-Mediterranean countries. In other cases, RC frame structures were basically designed only to gravity loads because of the lack of seismic codes with modern design criteria and/or detailing rules. This motivated the authors to design a retrofitting measure for the case-study structure, afterwards evaluating its impact on structural robustness in accordance with a multi-hazard approach.

According to previous studies (*e.g.*, [67]), local strengthening of RC frame structures based on FRP systems can be an effective strategy to mitigate seismic risk. Therefore, frame members prone to shear failure were supposed to be strengthened with CFRP sheets with single or multiple plies depending on the type and location of the member to be retrofitted. The selected CFRPs had the following properties: weight per unit area w_f = 1200 g/m^2; equivalent thickness of dry fabric t_f = 0.666 mm; effective area per unit width A_f = 666.4 mm^2/mm; tensile strength f_f = 4.9 GPa; ultimate tensile force per unit width F_f = 3265 kN/m; Young's modulus E_f = 252 GPa; and ultimate strain ε_{fu} = 2%.

FRP strengthening systems were designed according to CNR-DT 200R1/2013 guidelines [68], resulting in single-ply CFRP wraps for beams and multi-ply confinement systems for columns. More specifically, CFRP sheets around columns consisted of 5 plies at the ground floor, 3 plies at the second floor, 2 plies at the third floor, and a single ply at the last two floors. DCRs outlined in Tables 6 and 7 show that the retrofitting system was able to solve the issue of shear failure in beams and columns, respectively. Indeed, DCR was found to be lower than unity in all frame members.

Table 6. Shear demand-to-capacity ratios of beams after retrofitting.

Floor level	Beam span											
	Mass profile						Mode profile					
	A	B	C	D	E	F	A	B	C	D	E	F
1	0.83	0.79	0.80	0.80	0.79	0.80	0.79	0.77	0.78	0.79	0.79	0.81
2	0.68	0.64	0.63	0.62	0.60	0.60	0.82	0.77	0.76	0.74	0.73	0.72
3	0.64	0.60	0.59	0.57	0.55	0.54	0.73	0.67	0.65	0.64	0.62	0.61
4	0.48	0.47	0.46	0.45	0.43	0.42	0.56	0.53	0.52	0.50	0.48	0.47
5	0.35	0.33	0.33	0.32	0.32	0.29	0.40	0.36	0.35	0.35	0.35	0.32

Table 7. Shear demand-to-capacity ratios of columns after retrofitting.

Floor level	Column line													
	Mass profile							Mode profile						
	1	2	3	4	5	6	7	1	2	3	4	5	6	7
1	0.54	0.91	0.92	0.95	0.97	0.99	0.92	0.41	0.80	0.84	0.88	0.92	0.96	0.87
2	0.48	0.97	0.93	0.91	0.89	0.87	0.39	0.52	0.99	0.98	0.96	0.94	0.93	0.44
3	0.39	0.82	0.77	0.73	0.69	0.65	0.43	0.47	0.95	0.90	0.86	0.82	0.78	0.51
4	0.28	0.65	0.62	0.59	0.56	0.53	0.33	0.41	0.83	0.79	0.74	0.70	0.67	0.41
5	0.01	0.34	0.33	0.31	0.30	0.26	0.24	0.07	0.47	0.44	0.41	0.39	0.34	0.26

The impact of seismic retrofitting on structural robustness was significant. PDA under removal of corner column (scenario A1) highlighted the first shear failure at a vertical drift $\theta = 13.6\%$, resulting in a peak load multiplier higher than unity ($\alpha_{max} = 1.02$), as shown in Figure 16a. That was a major achievement, recalling that the as-built structure suffered the first shear failure at $\theta = 0.03\%$, corresponding to $\alpha_{max} = 0.33$. PDA results confirm a higher robustness level of the structure to internal column removal (scenario A2) after seismic retrofitting (Fig. 16b). In that scenario, the first shear failure occurred at $\theta = 1.0\%$ and $\alpha_{max} = 1.18$, indicating again an increase in both displacement and load capacity of the retrofitted structure. In as-built conditions, PDA under scenario A2 highlighted the first shear failure at $\theta = 0.3\%$ and $\alpha_{max} = 0.48$.

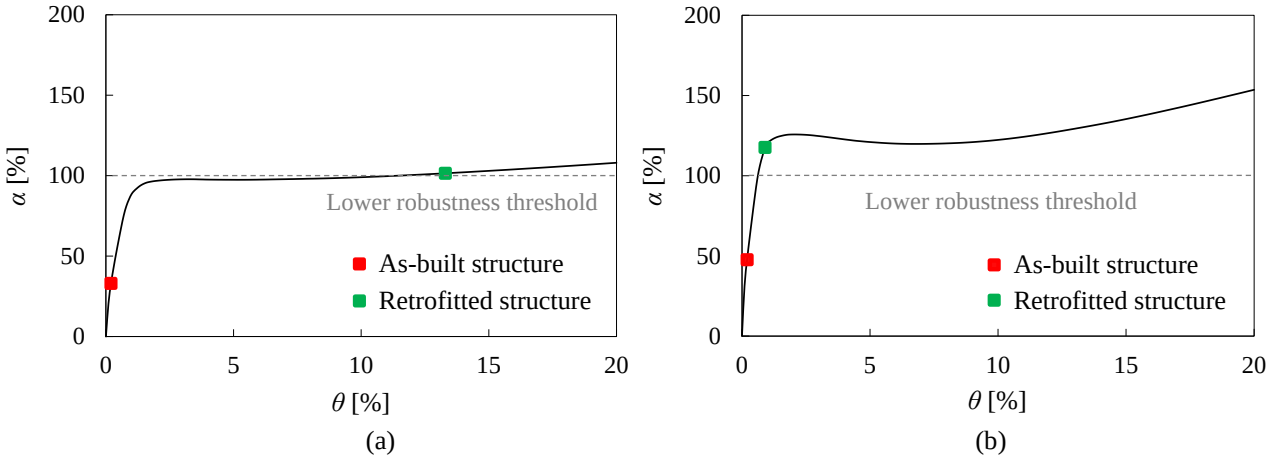

Figure 16. Impact of seismic retrofitting on structural robustness: (a) scenario A1; (b) scenario A2.

Based on analysis results, seismic retrofitting allowed the structure to develop a satisfactory level of robustness to both corner and central column-removal scenarios, as indicated by a peak load capacity higher than design gravity load (*i.e.*,

$\alpha_{max} > 1$).

5.2. Sensitivity to beam span length and shear strength of strengthening system

Several researchers investigated the influence of FRPs on the progressive collapse resistance of RC buildings through parametric analysis. Various variables were considered, such as the fibre type, installation technique, and fibre warping. The influence of glass fibre-reinforced polymers (GFRPs) on RC beam–slab sub-assemblages under corner column removal was analysed by Feng *et al.* [69], who investigated two different application techniques. That study showed that a higher load-carrying capacity could be obtained through the use of Near-Surface-Mounted GFRP bars with respect to the externally bonded reinforcement method. Qian *et al.* [69] studied two different application schemes for CFRP laminates on flat slabs. The application of the fibres at 45°–135° performed slightly better compared to that placed at 0–90°. Either way, the difference in load-carrying capacity between the two schemes was small, and Qian *et al.* [69] suggested the use of the last method in practice due to its easier application, deformation behaviour, and ductility. Yang *et al.* [70] analysed the effectiveness of basalt fibre-reinforced polymer (BFRP) bars and the effect of some parameters on the progressive collapse capacity of RC frames, founding a key role of BFRP bars in collapse resistance. Yang *et al.* [70] assessed the dynamic increase factor (*DIF*) of collapse load through the energy conservation method, highlighting $DIF = 2$ and $1.44 \leq DIF \leq 2$ in case of non-prestressed and prestressed frame structures reinforced with BFRP bars, respectively. In addition, the robustness of sub-assemblages increased as the span to depth ratio of beams decreased. Kim *et al.* [71] experimentally investigated the influence of anchorage techniques by varying the geometry and amount of CFRP materials on ten beam specimens. That study demonstrated that the full strength of CFRP sheets on the side faces could be achieved only by a combination of CFRP anchors and U-wraps. Additionally, Liu *et al.* [72] performed experimental tests to investigate the use of CFRP strip cables to retrofit a three-storey RC frame under sudden removal of two side-middle columns. Tests were performed considering the use of CFRP cable at all stories and at a single-story only. The tests demonstrated the effectiveness of the retrofit strategy in both cases, highlighting that reinforcement at a single storey can significantly affect the progressive collapse resistance of the entire structure.

The present study expands the current knowledge on the effectiveness and design of FRP-based retrofit strategies for progressive collapse by performing a parametric analysis on two critical properties of the structure and retrofitting system. Such parameters are the beam span length L_b of the case study structure and shear resistance of the strengthening system. Indeed, L_b can be a key geometric property for both earthquake resistance and progressive collapse capacity of a frame structure. Variations in L_b can result in either small or large variations in seismic performance, depending on whether the RC frame structure suffers soft-storey mechanisms or develops a global collapse mechanism, respectively. By contrast, L_b is expected to have always a strong impact on progressive collapse resistance and robustness. Therefore, a combined checking of the effects of L_b on both seismic safety and robustness is of special interest in this study.

Variations in shear capacity of the local strengthening system allows a generalization of this study to other types of retrofitting solutions, which are not necessarily based on the type of FRPs considered in previous sections of this paper. The sensitivity of the structural performance to shear capacity of the strengthening system is also expected to be rather high, as it can also affect the global behaviour of the structure under a progressive collapse scenario. The parametric analysis presented below was performed under corner column removal, *i.e.*, scenario A1, which has been previously found to be the worst scenario for the case-study structure.

L_b was varied between 4 m and 6 m, with step of 0.5 m, reproducing the beam span lengths that are most frequently observed in cast-in-place, European RC buildings. Hence, four span lengths were considered in addition to that of the reference structure (*i.e.*, $L_b = 5$ m), developing as many additional models of the frame structure. The performance of each model was thus assessed according to the methodology described in previous sections, hence first evaluating the seismic performance through pushover analysis. Afterwards, local strengthening system was designed to avoid brittle shear failures and was checked against column removal to assess the impact on progressive collapse resistance.

Figures 17a and 17b show variations of pushover curves in the acceleration–displacement plane under varying L_b, considering mode and mass force profiles, respectively. Given that the structure developed a soft-storey mechanism, the beam span length slightly influenced the displacement capacity while affecting more the peak lateral resistance as shown by variations in S_a.

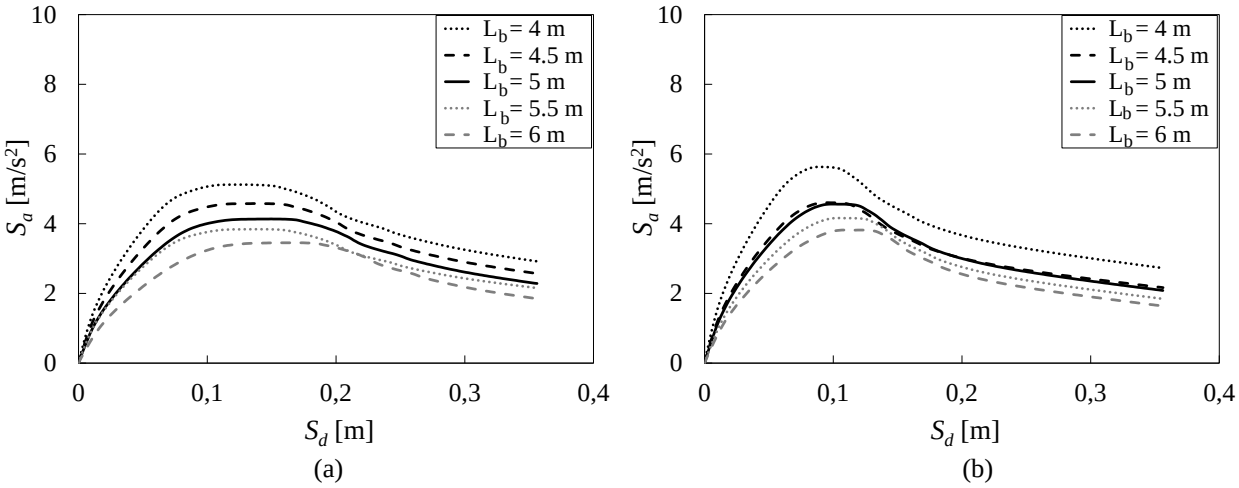

Figure 17. Pushover curves of case-study structure under varying beam span length: (a) mode force profile; (b) mass force profile.

Based on the output of seismic performance assessment, the local strengthening system was re-designed according to CNR-DT 200R1/2013 guidelines [68] to avoid brittle failures in beams and columns. Single-ply CFRPs were sufficient for beams belonging to all floor levels, exception made for the structure with longer beams, *i.e.*, L_b = 6 m. In that case, CFRP sheets consisted of two plies at each floor level. Dealing with columns, as L_b ranged from 4 m to 5 m, the same configuration of CFRP sheets was found, namely, 5 plies at the ground floor, 3 plies at the second floor, 2 plies at the third floor and a single ply at the last two floors. As L_b increased to 5.5 m, a similar result was found, with the exception of the ground floor in which 4 plies were used. When the beam span length was 6 m, a larger number of CFRP sheets that exceeds code limits (*i.e.*, 6 plies) was required, so the local strengthening system selected in previous cases did not allow avoiding brittle failures under seismic actions.

The influence of the beam span length on progressive collapse resistance of the as-built structure was also evaluated through PDA. Figure 18 shows that an increase in the beam span length produced a significant decrease in terms of robustness. As L_b changed from 4 m to 6 m, the maximum load multiplier α_{max} reduced from 1.87 to 0.71, indicating that the structure gradually reached a geometric configuration that is not sufficiently robust. Moreover, it can be observed that, in cases of L_b = 5.5 m and L_b = 6 m, local retrofit strategies aimed at the increase of rotational capacity at beam ends do not allow reaching the required progressive collapse resistance against design gravity loads. In addition, the increase in L_b produces brittle failures at smaller values of load multiplier, *e.g.*, α_{max} = 0.4 and α_{max} = 0.29 under L_b = 4 m and L_b = 6 m, respectively.

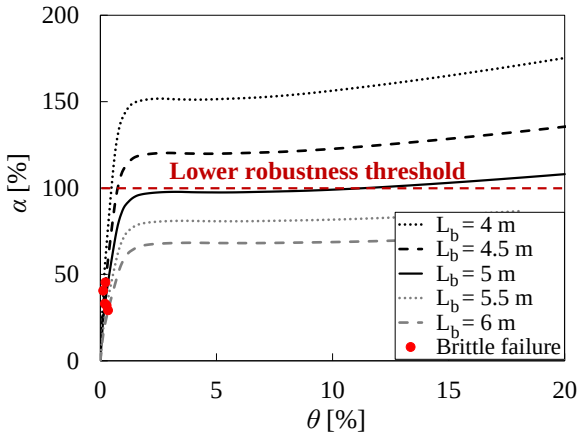

Figure 18. Dimensionless capacity curves under varying beam span length and identification of first shear failure.

After the CFRP design was carried out, PDA was carried out for all the considered values of L_b to assess the influence and effectiveness of the seismic retrofit measure on the progressive collapse resistance. Analysis results in Figure 19

underline the effectiveness of the strengthening intervention under L_b ranging between 4 m and 5 m. In cases of L_b equal to 4 m and 4.5 m, Figure 19 shows that the first brittle failures were identified at higher α-values, which were equal to 1.2 and 1.15, respectively. This emphasises the increase in ultimate load capacity compared to the previous case (as-built structure), in which α_{max} corresponding to brittle failures was found to be 0.40 and 0.45 under L_b equal to 4 m and 4.5 m, respectively. However, it is observed that, for those geometric configurations, the progressive collapse resistance was achieved without the activation of catenary actions and shorter beams induced brittle failures at lower values of drift θ. In cases of L_b equal to 5.5 m and 6 m, the structure itself does not allow the selected local retrofit strategy to improve robustness, because the pushdown curves does not reach the lower robustness thresholds (corresponding to α = 1) even at very large drifts. Therefore, such results underline the existence of some structural configurations where local strengthening can be an effective solution to improve seismic safety without necessarily producing significant benefits in terms of robustness.

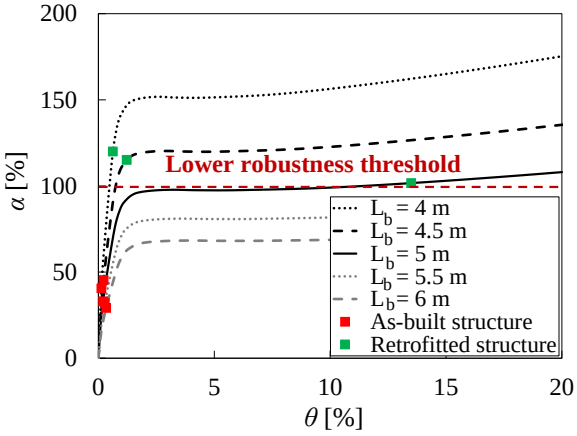

Figure 19. Impact of seismic retrofitting on structural robustness under varying beam span length.

Successively, the impact of variations in shear strength of the strengthening system at beam ends, V_{rdf}, was investigated. Such variations were set to ±10% and ±20%. This part of sensitivity analysis was performed on the structure with 4 m ≤ L_b ≤ 5 m due to the lack of structural robustness in the other two cases. Figure 20 shows the results of such a parametric analysis, using green squares to identify brittle failures reached by the structure retrofitted through the CFRP system presented in Section 5.1. In addition, other two types of markers are used in Figure 20: *(i)* blue and pink dots are related to the achievement of the first brittle failure in case of shear strength reduction ΔV_{rdf} = –10% and ΔV_{rdf} = –20%, respectively; *(ii)* yellow and purple rhombuses indicate the first brittle failure reached in case of shear strength amplification ΔV_{rdf} = +10% and ΔV_{rdf} = +20%, respectively.

In the case of structures with L_b equal to 4 m and 5 m, similar results were found after shear strength reduction of the strengthening system, as demonstrated by the overlapping of pink and blue dots. The first brittle failure occurred at α_{max} = 1.04 and α_{max} = 0.91 in case of L_b equal to 4 m and 5 m, respectively. A more significant difference can be observed on the structure with L_b = 4.5 m where the first brittle failure occurred at α_{max} = 1.08 and α_{max} = 0.95 under ΔV_{rdf} = –10% and ΔV_{rdf} = –20%, respectively. An amplification of shear strength led to an increase of load multiplier corresponding to the achievement of the first brittle failure. Specifically, ΔV_{rdf} = +10% induced α_{max} equal to 1.3, 1.16 and 1.06, under L_b equal to 4 m, 4.5 m and 5 m, respectively. The beneficial effect of local shear strengthening was even higher when assuming shear strength amplification ΔV_{rdf} = +20%, which resulted in α_{max} equal to 1.42 and 1.23 under L_b equal to 4 m and 4.5 m, respectively. In all cases where the first brittle failure was identified at low-to-moderate drift levels (i.e., $\theta \leq$ 5%), the structure was not able to develop catenary action. The opposite was found in the structure with L_b equal to 4.5 m and 5 m, where local strengthening at beam ends produced a significantly larger inelastic deformation capacity, developing the catenary action at drifts larger than approximately 10%. Nevertheless, local seismic strengthening can be an effective solution for robustness provided that it allows the structure to resist the design gravity loads after colum loss, hence reaching or exceeding the lower robustness threshold.

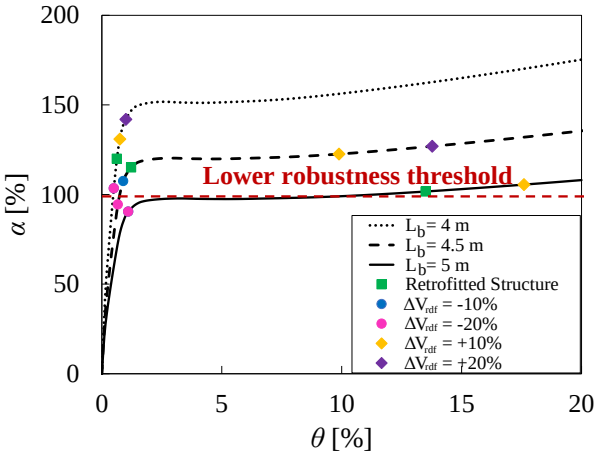

Figure 20. Sensitivity of brittle failure occurrence and corresponding load multiplier to shear capacity of local strengthening system.

6. Conclusions

In this study, a benchmark RC frame structure designed only to gravity loads was assessed under seismic actions and notional column-removal scenarios, before and after retrofitting. A fibre-based FE model of the structure was developed in OpenSees [55] and compared to a similar model that was implemented and analysed in SeismoStruct [60]. Seismic and progressive collapse assessments were based on nonlinear incremental static analyses with displacement control, namely, pushover and pushdown analysis procedures. Pushdown capacity curves derived in this study were compared to those presented in a previous paper [54] according to incremental dynamic analysis, allowing a structure-specific assessment of dynamic amplification factor for gravity loads. That factor was then used to evaluate the progressive collapse capacity of the as-built structure via pushdown analysis, investigating the mobilisation of arch and catenary resisting mechanisms under increasing maximum strain of longitudinal steel bars located within beams. The same structure was seismically assessed by means of pushover analysis, according to current code-based procedures. Both progressive collapse capacity and seismic performance of the structure were evaluated at global and local levels, hence identifying potential shear failures not explicitly considered in the fibre-based FE model. In the final istance a parametric analysis was performed in order to assess the variation of progressive collapse resistance to the change of some properties, both structural and of the materials.

This multi-hazard assessment study allows the following conclusions to be drawn:

- The ultimate steel strain affects the rotational capacity of beams above the removed column, with 10% or 20% strain allowing the development of catenary action and increasing the progressive collapse capacity of the structure.
- Local checks based on post-processing of pushdown and pushover analysis results provided evidence that both seismic safety and robustness of the structure can be significantly reduced due to the premature shear failures in beams and columns.
- Robustness enhancement can be effectively driven by seismic retrofitting based on CFRP strengthening, highlighting the importance of multi-hazard approaches for design, assessment and retrofit of structures.
- Variations in beam span length can produce significantly different effectiveness levels for CFRP strengthening, evidencing insufficient levels of robustness if beam span length is higher than 5 m. In those situations, local seismic strengthening may be ineffective to significantly improve robustness, hence calling for other retrofitting options that, for instance, can provide alternative load paths.
- Significant beneficial effects of local seismic strengthening on robustness (in terms of load-bearing capacity and, in some cases, inelastic deformation capacity) can result from 10%–20% amplifications in shear strength at beam ends, significantly delaying the occurrence of brittle failures. In case of shorter beams with span length between 4 m and 4.5 m, a shear strength reduction of the local seismic strengthening system can still ensure a sufficient level of robustness. Such findings may also be used to drive design of other systems for local seismic-robustness strengthening that rely on the improvement of shear resistance at beam ends.

The outcomes of this study create a basis for future research developments on the interaction between seismic resistance

and structural robustness, which can support disaster risk mitigation and sustainability of the built environment. Further studies are needed to explore the impact of other seismic retrofit methods (*e.g.*, steel braces, RC walls, steel caging) on progressive collapse resistance and, reciprocally, the influence of different methods for robustness enhancement on earthquake resistance. Infill masonry walls should also be implemented in the structural model to assess their impact on seismic strengthening and robustness. Indeed, infill walls typically have a strong effect in terms of both stiffness and load-bearing capacity in both horizontal and vertical directions of the RC frame structure. It is also emphasised that this study focused on 2D frame systems, thus calling for future developments on 3D frames where other aspects such as the irregularity in plan and the selection of control point for pushover analysis should be taken in due consideration.

Acknowledgements
This study was supported by GRISIS project (Gestione dei Rischi e Sicurezza delle Infrastrutture a Scala regionale) funded by Regione Campania.

References

1. Pearson C, Delatte N. Ronan Point apartment tower collapse and its effect on building codes. J Perform Constr Facil 2005; 19: 172–177.
2. Kazemi-Moghaddam A, Sasani M. Progressive collapse evaluation of Murrah Federal Building following sudden loss of column G20. Eng Struct 2015; 89: 162–171.
3. Bažant Z, Verdure M. Mechanics of progressive collapse: Learning from World Trade Center and building demolitions. J Eng Mech. 2007; 133: 308–319.
4. Gross JL, McGuire W. Progressive collapse resistant design. J Struct Eng 1983; 109: 1–15.
5. Adam JM, Parisi F, Sagaseta J, Lu X. Research and practice on progressive collapse and robustness of building structures in the 21st century. Eng Struct 2018; 173: 122–149.
6. Sadek F, Main JA, Lew HS, Robert SD, Chiarito VP, El-Tawil S. An experimental and computational study of steel moment connections under a column removal scenario. NIST Technical Note 1669, National Institute of Standards and Technology, Gaithersburg, MD; 2010.
7. Lew HS, Bao Y, Sadek F, Main JA, Pujol S, Sozen MA. An experimental and computational study of reinforced concrete assemblies under a column removal scenario. NIST Technical Note 1704, National Institute of Standards and Technology, Gaithersburg, MD; 2011.
8. Zandonini R, Baldassino N, Freddi F. Robustness of steel-concrete flooring systems. An experimental assessment. Stahlbau 2014; 83(9): 608–613.
9. Ren P, Li Y, Lu X, Guan H, Zhou Y. Experimental investigation of progressive collapse resistance of one-way reinforced concrete beam–slab substructures under a middle-column-removal scenario. Eng Struct 2016; 118: 28–40.
10. Lu X, Lin K, Li Y, Guan H, Ren P, Zhou Y. Experimental investigation of RC beam-slab substructures against progressive collapse subject to an edge-column-removal scenario. Eng Struct 2017; 149: 91–103.
11. Zandonini R, Baldassino N, Freddi F, Roverso G. Steel-concrete composite frames under the column loss scenario: An experimental study. J Constr Steel Res 2019; 162: 105527.
12. Adam JM, Buitrago M, Bertolesi E, Sagaseta J, Moragues JJ. Dynamic performance of a real-scale reinforced concrete building test under a corner-column failure scenario. Eng Struct 2020; 210: 110414.
13. Buitrago M, Bertolesi E, Sagaseta J, Calderón PA, Adam JM. Robustness of RC building structures with infill masonry walls: Tests on a purpose-built structure. Eng Struct 2021; 226: 111384.
14. Marjanishvili SM. Progressive analysis procedure for progressive collapse. J Perform Constr Facil 2004; 18: 79–85.
15. Parisi F., Augenti N. Influence of seismic design criteria on blast resistance of RC framed buildings: A case study. Eng Struct 2012; 44: 78–93.
16. Brunesi E, Nascimbene R, Parisi F, Augenti N. Progressive collapse fragility of reinforced concrete framed structures through incremental dynamic analysis. Eng Struct 2015; 104: 65–79.
17. Tsai MH, Lin BH. Investigation of progressive collapse resistance and inelastic response for an earthquake-resistant RC building subjected to column failure. Eng Struct 2008; 30: 3619–3628.
18. Dat PX, Hai TK, Jun Y. A simplified approach to assess progressive collapse resistance of reinforced concrete framed structures. Eng Struct 2015; 101: 45–57.
19. Izzuddin BA, Vlassis AG, Elghazouli AY, Nethercot DA. Progressive collapse of multi-storey buildings due to sudden column loss — Part I: Simplified assessment framework. Eng Struct 2008; 30: 1308–1318.
20. Feng DC, Xie SC, Deng WN, Ding ZD. Probabilistic failure analysis of reinforced concrete beam-column sub-assemblage under column removal scenario. Eng Fail Anal 2019; 100: 381–392.

21. Dimopoulos C, Freddi F, Karavasilis TL, Vasdravellis G. Progressive collapse of self-centering moment resisting frames. Eng Struct 2020; 208: 109923.
22. Li Y, Lu X, Guan H, Ye L. An improved tie force method for progressive collapse resistance design of reinforced concrete frame structures. Eng Struct 2011; 33: 2931–2942.
23. Ellingwood BR. Building design for abnormal loads and progressive collapse. Comp Aid Civil Infrastruct Eng 2005; 20: 194–205.
24. Gross JL, McGuire W. Progressive collapse resistant design. J Struct Eng 1983; 109(1): 1–15.
25. Unified facilities criteria (UFC). UFC 4-023-03: Design of structures to resist progressive collapse (Rev. 3). Washington, DC: US Department of Defence; 2016.
26. CEN. EN 1990: Eurocode – Basis of structural design. Brussels: Comité Européen de Normalisation; 2002.
27. General Services Administration (GSA). Alternative path analysis and design guidelines for progressive collapse resistance. Washington, DC: Office of Chief Architects; 2013.
28. Augenti N, Parisi F. Learning from construction failures due to the 2009 L'Aquila, Italy, earthquake. J Perform Constr Facil 2010; 24(6): 536–555.
29. Freddi F, Novelli V, Gentile R, Veliu E, Andonov A, Andreev S, Greco F, Zhuleku E. Observations from the 26th November 2019 Albania earthquake: The Earthquake Engineering Field Investigation Team (EEFIT) mission. Bull Earthq Eng 2021.
30. Ghosh J, Sood P. Consideration of time-evolving capacity distributions and improved degradation models for seismic fragility assessment of aging highway bridges. Reliab Eng Syst Saf 2016; 154: 197–218.
31. Freddi F, Tubaldi E, Ragni L, Dall'Asta A. Probabilistic performance assessment of low-ductility RC frames retrofitted with dissipative braces. Earthq Eng Struct Dyn 2013; 42(7): 993–1011.
32. Gioiella L, Tubaldi E, Gara F, Dezi L, Dall'Asta A. Modal properties and seismic behaviour of buildings equipped with external dissipative pinned rocking braced frames. Eng Struct 2018, 172: 807–819.
33. Freddi F, Tubaldi E, Zona A, Dall'Asta A. Seismic performance of dual systems coupling moment-resisting frames and buckling-restrained braced frames. Earthq Eng Struct Dyn 2021; 50(2): 329–353.
34. Freddi F, Ghosh J, Kotoky N, Raghunandan M. Device uncertainty propagation in low-ductility RC Frames retrofitted with BRBs for seismic risk mitigation. Earthq Eng Struct Dyn 2021. DOI: 10.1002/eqe.3456
35. Kim Y, Lim SA, Park HS. Optimal seismic retrofit method for reinforced concrete columns with wing walls. Eng Struct 2020; 210: 11039.
36. Maheri M, Sahebi A. Use of steel bracing in reinforced concrete frames. Eng Struct 1997; 19: 1018–1024.
37. Pampanin S, Bolognini D, Pavese A. Performance-based seismic retrofit strategy for existing reinforced concrete frame systems using fiber-reinforced polymer composites. J Compos Constr 2007; 11(2): 211–226.
38. Pohoryles DA, Melo J, Rossetto T, Varum H, Bisby L. Seismic retrofit schemes with FRP for deficient RC beam-column joints: State-of-the-art review. J Compos Constr 2019, 23(4): 03119001.
39. Ozcan O, Binici B, Ozcebe G. Seismic strengthening of rectangular reinforced concrete columns using fiber reinforced polymers. Eng Struct 2010; 32: 964–973.
40. Li S, Shan S, Zhang H, Li Y. Rapid retrofit of reinforced concrete frames after progressive collapse to increase sustainability. Sustainability 2019; 11: 4195.
41. Jinkoo K, Woo-Seung S. Retrofit of RC frames against progressive collapse using prestressing tendons. Struct Design Tall Spec Build 2013; 22: 349–361.
42. Shayanfar M, Bigonah M, Sobhani D, Zabihi-Samani M. The effectiveness investigation of new retrofitting techniques for RC frame against progressive collapse. Civil Eng J 2018; 4(9): 2132–2142.
43. Orton S, Jirsa JO, Bayrak O. Carbon fiber-reinforced polymer for continuity in existing reinforced concrete buildings vulnerable to collapse. ACI Struct J 2009; 106(5): 608–616.
44. Qian K, Li B. Strengthening and retrofitting precast concrete buildings to mitigate progressive collapse using externally bonded GFRP strips. J Compos Constr 2019; 23(3): 04019018.
45. Qin W, Liu X, Xi Z, Huang Z, Al-Mansour A, Fernand M. Experimental research on the progressive collapse resistance of concrete beam-column sub-assemblages reinforced with steel-FRP composite bar. Eng Struct 2021; 233: 111776.
46. Li Y, Ahuja A, Padgett JE. Review of methods to assess, design for, and mitigate multiple hazards. J Perform Constr Facil 2012; 26(1): 104–117.
47. Lin KQ, Li Y, Lu X, Guan H. Effects of seismic and progressive collapse designs on the vulnerability of RC frame structures. J Perform Constr Facil 2016; 31(1): 04016079.
48. Brunesi E, Parisi F. Progressive collapse fragility models of European reinforced concrete framed buildings based on pushdown analysis. Eng Struct 2017; 152: 579–596.

49. Parisi F, Scalvenzi M. Progressive collapse assessment of gravity-load designed European RC buildings under multi-column loss scenarios. Eng Struct 2020; 209: 110001.
50. Feng P, Qiang H, Qin W, Gao M. A novel kinked rebar configuration for simultaneously improving the seismic performance and progressive collapse resistance of RC frame structures. Eng Struct 2017; 147: 752–767.
51. Lin K, Lu X, Li Y, Guand H. Experimental study of a novel multi-hazard resistant prefabricated concrete frame structure. Soil Dyn Earthq Eng 2019; 119: 390–407.
52. Lin K, Lu X, Li Y, Zhuo W, Guan H. A novel structural detailing for the improvement of seismic and progressive collapse performances of RC frames. Earthq Eng Struct Dyn 2019; 48: 1451–1470.
53. CEN. EN 1992-1-1:2004: Eurocode 2 – Design of concrete structures. Part 1.1: General rules and rules for buildings. Brussels: Comité Européen de Normalisation; 2004.
54. Parisi F, Scalvenzi M, Brunesi E. Performance limit states for progressive collapse analysis of reinforced concrete framed buildings. Struct Concrete 2019; 20(1): 68–84.
55. McKenna F, Fenves GL, Scott MH. OpenSees — Open system for earthquake engineering simulation. Berkeley: Pacific Earthquake Engineering Research (PEER) Center, University of California Berkeley; 2004.
56. Eren N, Brunesi E, Nascimbene R. Influence of masonry infills on the progressive collapse resistance of reinforced concrete framed buildings. Eng Struct 2019; 178: 375–394.
57. Buitrago M, Bertolesi E, Sagaseta J, Calderon PA, Adam JM. Robustness of RC building structures with infill masonry walls: Tests on a purpose-built structure. Eng Struct 2021; 226: 111384.
58. Di Sarno L, Freddi F, D'Aniello M, Kwon OS, Wu JR, Gutiérrez-Urzúa LF, Landolfo R, Park J, Palios X, Strepelias E. Assessment of existing steel frames: Numerical study, pseudo-dynamic testing and influence of masonry infills. J Constr Steel Res 2021; 185: 106873.
59. Scott BD, Park R, Priestley MJN. Stress–strain behavior of concrete confined by overlapping hoops at low and high strain rates. ACI J 1982; 79(1): 13–27. Available from: http://opensees.berkeley.edu.
60. Seismosoft. SeismoStruct — A computer program for static and dynamic nonlinear analysis of framed structures. 2016. Available from: www.seismosoft.com.
61. Brunesi E, Nascimbene R. Extreme response of reinforced concrete buildings through fiber force-based finite element analysis. Eng Struct 2014; 69: 206–215.
62. CEN. EN 1998-1:2004: Eurocode 8 – Design of structures for earthquake resistance. Part 1: General rules, seismic actions and rules for buildings. Brussels: Comité Européen de Normalisation; 2004.
63. Parisi F, Adam JM, Sagaseta J, Lu X. Review of experimental research on progressive collapse of RC structures. In: Augenti N, Jurina L (eds). Ingegneria Forense, Crolli, Affidabilità Strutturale e Consolidamento — Atti del Convegno IF CRASC '17. Volume 2. Palermo: Flaccovio Editore, 2017; p. 265–276.
64. Biskinis DE, Roupakias GK, Fardis MN. Degradation of shear strength of reinforced concrete members with inelastic cyclic displacement. ACI Struct J 2004; 101(6): 773–783.
65. MIT. DM 17.01.2018: Norme tecniche per le costruzioni. Rome: Italian Ministry for Infrastructure and Transportation; 2018.
66. CEN. EN 1998-1:2004: Eurocode 8 – Design of structures for earthquake resistance. Part 1: General rules, seismic actions and rules for buildings. Brussels: Comité Européen de Normalisation; 2004.
67. Frascadore R, Di Ludovico M, Prota A, Verderame GM, Manfredi G, Dolce M, Cosenza E. Local strengthening of reinforced concrete structures as a strategy for seismic risk mitigation at regional scale. Earthq Spectra 2019; 31(2): 1083–1102.
68. CNR. CNR-DT 200R1/2013: Guide for the design and construction of externally bonded FRP systems for strengthening existing structures. Rome: National Research Council of Italy; 2013.
69. Feng P, Qiang H, Ou X, Qin W, Yang J. Progressive collapse resistance of GFRP-strengthened RC beam–slab subassemblages in a corner column–removal scenario. J Compos Constr 2019; 23(1): 04018076.
70. Qian K, Li B. Strengthening and retrofitting of RC flat slabs to mitigate progressive collapse by externally bonded CFRP laminates. J Compos Constr 2013; 17(4): 554–565.
71. Yang T, Han Z, Deng N, Chen W. Collapse responses of concrete frames reinforced with BFRP bars in middle column removal scenario. Appl Sci 2019; 9: 4436.
72. Kim I, Jirsa JO, Bayrak O. Anchorage of carbon fiber-reinforced polymer on side faces of reinforced concrete beams to provide continuity. ACI Struct J 2013; 110(6): 1089–1098.
73. Liu T, Xiao Y, Yang J, Chen BS. CFRP strip cable retrofit of RC frame for collapse resistance. J Compos Constr 2017; 21(1): 04016067.